Food Chemistry 461 (2024) 140817

Contents lists available at ScienceDirect

Food Chemistry

journal homepage: www.elsevier.com/locate/foodchem

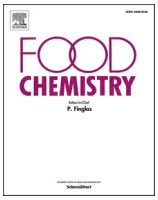

Structural evolution of maize starches with different amylose content during pasting and gelation as evidenced by Rapid Visco Analyser

Ke Guo [a,b,c], Yu Tian [c], Dagmara Podzimska-Sroka [d,e], Jacob Judas Kain Kirkensgaard [f,g], Klaus Herburger [h], Kasper Enemark-Rasmussen [i], Tue Hassenkam [j], Bent Larsen Petersen [c], Andreas Blennow [c,d,*], Yuyue Zhong [a,c,*]

[a] Department of Food Science and Nutrition, The Hong Kong Polytechnic University, Hung Hom, Kowloon, Hong Kong, China
[b] Institute of Food Crops, Jiangsu Academy of Agricultural Sciences, Nanjing 210014, China
[c] Department of Plant and Environmental Sciences, Copenhagen Plant Science Center, Faculty of Science, University of Copenhagen, Denmark
[d] PlantCarb ApS, Hørsholm, Denmark
[e] Carlsberg Research Laboratory, Gamle Carlsberg Vej 10, DK-1799 Copenhagen V
[f] Department of Food Science, University of Copenhagen, DK-1958 Frederiksberg C, Denmark
[g] Niels Bohr Institute, Universitetsparken 5, 2100 København Ø, Denmark
[h] Institute of Biological Sciences, University of Rostock, Germany
[i] Department of Chemistry, Technical University of Denmark, DK-2800, Kemitorvet, Building, 207 Kgs. Lyngby, Denmark
[j] Globe Institute, University of Copenhagen, DK-1350 Copenhagen, Denmark

ARTICLE INFO

Keywords:
RVA
SEM
Gelation
Maize starch
Viscosity

ABSTRACT

This study examined multi-scale structural alterations of maize starches varying in amylose content during pasting and gelation, using Rapid Visco Analyser (RVA). At 50 °C, starch granules maintained their morphology with low viscosity. As the temperature increased to 95 °C, helical and crystal structures were destroyed, leading to granule swelling, distortion and porosity, as identified by Wide Angle X-ray Scattering and Fourier Transforms Infrared measurements at 90% moisture. This resulted in increased viscosity and the formation of a loose gel network structure. Subsequently, maintaining the temperature at 95 °C caused a decrease in viscosity as most granules disappeared, forming a reorganized flaky gel structure with larger pores. As the temperature decreased, gel porosity reduced. In high amylose content starch, the viscosity remained low and granules were partially gelatinized since the heating temperature was below the gelatinization temperature. This study is the first to detail starch multilevel structural dynamics during RVA gelatinization.

1. Introduction

Starch is among the most abundant polysaccharides in nature and composed of mainly linear α-1,4-linked amylose (AM) and the predominant amylopectin (AP), which has a α-1,4-linked backbone decorated with α-1,6-branched sidechains (Zhong et al., 2022). Combined, the two macromolecular structures intertwine into various assemblies, which include crystalline and amorphous lamellae, blocklets, concentric shells of growth rings and ultimately complete starch granules (Zhong et al., 2021). According to the different amylose content, starch can be divided into waxy, normal and high amylose starch (Zhong et al., 2022).

From an applied point of view, the pasting properties of starches are a key parameter for defining its performance as a thickener, gelation agent, and stabilizer (Mahmood, Kamilah, Shang, Sulaiman, & Ariffin, 2017). Rapid Visco Analyser (RVA) is the most commonly used instrument for analysing starch pasting properties, due to its high sensitivity, reproducibility of results, versality and the requirement of only small amounts of sample.The RVA procedure typically mimics the cooking process of starch-based systems when a starch/flour-water suspension is subjected to a heat-hold-cool-hold temperature cycle under constant shearing that is applied through a paddle (Balet, Guelpa, Fox, & Manley, 2019; Liu et al., 2019). A standardised RVA-mediated analysis of the pasting and gelation process in starch suspension is divided into five stages: (1) the initial stage, with a rotation rate of 960 rpm at 50 °C for 1 min; (2) the heating stage, heating to 95 °C at 160 rpm over 3 min 42 s; (3) the holding stage at 95 °C and 160 rpm for 2 min 30s; (4) the cooling

* Corresponding authors at: Department of Food Science and Nutrition, The Hong Kong Polytechnic University, Hung Hom, Kowloon, Hong Kong, China.
E-mail addresses: ab@plantcarb.com (A. Blennow), yuyuezhong93@163.com (Y. Zhong).

https://doi.org/10.1016/j.foodchem.2024.140817
Received 25 March 2024; Received in revised form 19 July 2024; Accepted 8 August 2024
Available online 10 August 2024

stage, cooling to 50 °C at 160 rpm over 3 min 48 s; and (5) the final holding stage at 50 °C and 160 rpm for 2 min (Balet et al., 2019).

Previous efforts in this area focused on the determination of starch pasting and viscous properties and their application in food and agricultural breeding field (Balet et al., 2019; Cozzolino, 2016). Additionally, it is well documented that, during gelatinization, starch granules first absorb water, then swell and partially disrupt in the second stage, accompanied by the gradual disruption of starch crystalline and granule structures, thus forming a paste. Finally, starch molecules reorganize and form new interactions, generating a gel with a porous structure (Balet et al., 2019; Chen et al., 2011; Wu, Ma, Fu, & Tang, 2022; Xu, Blennow, Li, Chen, & Liu, 2020). However, no systematic documentation on the structural changes occurring during starch gelatinization and its relationship with viscosity is currently available. For example, it is not precisely clear at what stage the starch structure changes and what precise structures that are generated, such as crystal structures and granule structures, and their relationship with pasting parameters. Also, certain differences due to different starch types are likely to exist. Notably, for a given RVA process, the amylose content is a key factor determining the starch pasting properties, in which higher amylose content usually shows a lower peak viscosity and higher peak time (Liu, Chen, Bie, Xie, & Zheng, 2021; Tian et al., 2022). However, there is no substantial experimental RVA-data on the starch structural changes occurring during the hydrothermal gelatinisation-gelation progression, which strongly limits our understanding of the starch gelation process. We hypothesized that the starch crystal structure was abolished prior to the rise in viscosity, and the gel network structure was related to the fragmentation of the particle structure and the amylose content.

In this study, waxy (WMS, high amylopectin), normal (NMS) and high amylose maize (HAMS) starches – all of which have different amylose contents – were chosen as model materials to investigate the multi-scale structural progression during the hydrothermal process using RVA. With this study we anticipated deep insights into the progression of starch swelling, gelatinization, gelation and short-term retrogradation, all of which are critical for directly informing and optimising applications in the starch food industry.

2. Materials and methods

2.1. Sample preparation

Waxy maize starch (WMS) was purchased from Cerestar-AKV I/S (Denmark), normal maize starch (Commercial Clinton 106) (NMS) was provided by Archer Daniels Midland (ADM, Decatur, IL), and high amylose maize starch (Gelose50) (HAMS) was provided from Australia (Penford Australia Ltd.). All of these samples were extracted with the same protocol to exclude the influence of lipids and proteins on gelatinization. The samples all showed high starch purity, with starch content exceeding 95% (Table. S1) as analysed by Megazyme Total Starch Assay Kit (K-TSTA). Previous studies demonstrate that starch concentration has a significant effect on RVA properties (Castanha, Rojas, & Augusto, 2021; Lu, Wang, Zhao, & Lu, 2008). Therefore, in this study, the RVA tests of all three types of starch were determined at the same concentration, securing consistency and reliability of the readout data. Differential Scanning Calorimetry (DSC) analysis also identified no lipid complexes (Fig. S1 and Table S1). The RVA trials were performed as follows: Starch (2.5 g) was suspended in 25 mL water and stirred at 960 rpm for the first 10 s and then at a constant speed of 160 rpm during the whole analysis. The starch suspension was first held at 50 °C for 1 min, then heated to 95 °C at a rate of 12 °C/min (3.75 min) and held for 2.5 min, and finally cooled down to 50 °C at a rate of 12 °C/min (3.75 min) and finally held for 1.4 min. The specific sampling time points were determined by pre-experiments (Fig. S2). At the given time-points, the procedure was immediately stopped, and the samples were snapfrozen in liquid nitrogen and lyophilized. The dry sample was divided into two parts, one part was ground for further analysis and the other part used for Scanning Electron Microscopy (SEM) analysis.

2.2. Chemicals and reagents

Amylopectin (10120) and LiBr (213225) were purchased from Sigma-Aldrich. Isoamylase (*E*-ISAMY) was obtained from Megazyme International Ireland Ltd. DMSO (1.01900.2500) was purchased from Avantor Company (UK). The other chemicals and reagents were of analytical grade and obtained from Sigma-Aldrich.

2.3. Molecular size distribution by size exclusion chromatography (SEC) analysis

The size distributions of branched and debranched starch were analysed as described before with minor modifications (Li, Prakash, Nicholson, Fitzgerald, & Gilbert, 2016; Tao, Li, Yu, Gilbert, & Li, 2019), using a SEC-triple detector array SEC-TDA (Viscotek, Malvern, UK) equipped with GRAM 1000 SEC columns (Polymer Standards Service GmbH, Mainz, Germany) connected to a refractive index detector (PN3140, PostNova Analytics, Landsberg, Germany). A series of pullulan and dextran standards (Polymer Standard Services, Mainz, Germany) with varying molecular weights ranging from 342 to 8.72×10^6 Da were used for calibration. For branched starch, 5 mg starch was dissolved in 1 mL Dimethyl sulfoxide / Lithium Bromide (DMSO/LiBr, 0.5% *w*/w, Avantor, UK) at 80 °C overnight and centrifuged at 8000 *g* for 5 min, the supernatant (50 μL) was injected into the SEC system after centrifugation. Elution was performed using DMSO/LiBr (0.5%, *w*/w) at a flow rate of 0.5 mL/min and a column temperature of 65 °C. For debranched starch, 5 mg starch was dissolved in 1 mL DMSO/LiBr (0.5% w/w, Avantor, UK) at 80 °C for 3 h, and anhydrous ethanol was added to precipitate starch. Next, samples were left in a fume hood to allow ethanol evaporation. 2 μL isoamylase (*E*-ISAMY, Megazyme) in 1 mL sodium acetate buffer (0.01 M, pH 4.0) were added to the samples and incubated at 40 °C for 3 h, followed by freeze-drying and then subjecting the samples to SEC analysis.

2.4. Morphological observation of starch

A starch granular suspension (1% (*w/v*) in 50% glycerol) was analysed with a polarized light microscope (Leica DM 5000B) under normal and polarized light. The morphology of the starch granules and gels were monitored at high resolution by Field Emission Scanning Electron Microscopy (FE-SEM) (FEI Quanta 200), after fixing and sputter-coating granules with gold (Zhong et al., 2022).

2.5. Wide-angle X-ray scattering (WAXS) analysis

The crystalline starch structure was analysed using a Nano-inXider instrument (Xenocs SAS, Grenoble, France) equipped with a Cu Kα source with a 1.54 Å wavelength according to our previous protocol (Zhong, Li, et al., 2021). The starch was equilibrated to 90% humidity against a saturated aqueous solution of NaCl for 2 weeks. Samples were sealed in 5–7 μm mica films and scanned from 2θ- 5° to 40° using 40 mA current, 40 kV voltage, and 0.1542 nm wavelength Cu Kα radiation. The relative crystallinity was calculated as the percentage of the crystalline peak area to total diffraction area in the range of 2θ- 5° to 40° (Zhong et al., 2021).

2.6. Small-angle X-ray scattering (SAXS) analysis

The starch nano-lamellar structure was analysed by a Nano-inXider instrument (Xenocs SAS, Grenoble, France) (Zhong et al., 2021). Starch powder was suspended with excess distilled water and placed at 4 °C overnight. The suspension was centrifuged at 5000 *g* for 5 min, the supernatant removed and the remaining suspension (0.7 mL) was placed in 1-mm-thick sample cells for further measurement. The date

processing and background subtraction were following by previous report (Zhong et al., 2020).

2.7. Attenuated total reflectance-Fourier transforms infrared (ATR-FTIR) analysis

The short-range ordered structure was measured following our previous method (Guo et al., 2019). Spectral data were acquired using a Bomem MB100 FTIR spectrometer (ABB-Bomem, Quebec, Canada) equipped with a Golden gate attenuated total reflectance (ATR) accessory. Since the moisture content has a notable influence on the FTIR spectra (Shivaraju, Appukuttan, & Kumar, 2018), a consistent moisture content was applied to all samples; 50 mg of dry starch powder was mixed with 50 μL of deionized water in a 2 mL centrifuge tube, amalgamated well, and equilibrated at 4 °C overnight. The samples were scanned 64 times from 4000 to 800 cm^{-1} with a resolution of 2 cm^{-1}, and water was used as a blank to subtract the background. The spectral baseline was selected as 1200–800 cm^{-1}, the half-peak width was 19 cm^{-1}, the enhancement factor was 1.9, and the spectrum was deconvoluted using OMNIC software.

2.8. Solid-state ^{13}C nuclear magnetic resonance (SS-NMR) analysis

SS-NMR analysis of starch was performed using a Bruker AV-300 spectrometer as described before (Zhong, Li, et al., 2021). Starch suspension (1% *w/v*) was heated at 95 °C for 30 min to prepare amorphous standard samples (Tan, Flanagan, Halley, Whittaker, & Gidley, 2007). Before test, all the samples dried in 40 °C overnight, approximately 300 mg starch was packed in a 4-mm diameter rotor and the rotor spun at 5–6 kHz at the magic angle (54.7°). The 90° pulse width was 5 μs and a contact time of 1 ms was used for all starch samples with a recyle delay of 5 s. At least 2400 scans were accumulated for each spectrum with spectral width of 38 kHz, with an acquisition time of 3 ms. The relative content of single helix (102–103 ppm), double helix (99–101 ppm) and amorphous region were calculated according to a previous report (Tan et al., 2007). The NMR spectrum of amorphous starch was matched to the intensity of starch residues at 84 ppm, and was subtracted to produce the ordered subspectrum. The areas of the amorphous and ordered subspectra relative to the total area of spectrum yielded the percentages of amorphous and ordered components, respectively.

2.9. Rheological properties of starch

The dynamic rheological analysis of NMS, WMS and HAMS starch gels was analysed by Discovery HR-3 Rheometer (TA Instruments, New Castle, USA) at room temperature (Ding, Blennow, & Zhong, 2024). WMS and NMS were gelatinized at 100 °C for 30 min, and HAMS was gelatinized at 130 °C under pressure for 30 min. The starch concentration is 5%. Frequency sweeps were carried out from 0.01 to 100.00 Hz. The storage and loss modulus were selected at 1 Hz in the linear viscoelastic region.

2.10. Granule and agglomerate size distribution

The granule size distribution of starch was measured by a laser diffraction particle size analyser (Mastersizer 3000, Malvern, UK) (Guo et al., 2019). The starch-water suspension was stirred at 2000 rpm, and the measurement started when the obscuration of the suspension reached 10%.

2.11. Atomic force microscopy (AFM) analysis

The lyophilized and ground samples were scanned using an Asylum Research MFP-3D AFM instrument following a previous report (Ridout, Gunning, Parker, Wilson, & Morris, 2002). A standard silicon cantilever probe was used in tapping mode. Samples were scanned at room temperature with a drive amplitude 22 mV and drive frequency 76.5 kHz. The scanning ranges of raw and samples collected at 2.5 min were 5 × 5 μm while 3.5 min and 6 min samples were 2 × 2 μm. To mitigate surface damage, the spring constant was 1 N/m and the scan rate was 1.0 Hz. Images were collected by MFP3D software.

2.12. Statistical analysis

All experiments were carried out in triplicate, and data were presented as average value ± standard error. Determination of significant difference between average values and Pearson's correlation analysis were done in SPSS 20.0, followed by Duncan's post hoc test at 95% confidence level ($p < 0.05$).

3. Results and discussion

3.1. Molecular structure of starch

The molecular structures of WMS, NMS and HAMS were analysed by size-exclusion chromatography (SEC) (Table S2 and Fig. S3). For branched starch, SEC chromatograms (Fig. S3A) can be divided into two regions: region I ($R_h \leq 55$ nm) and region II ($R_h > 55$ nm), which are always recognized as AM and AP fraction, respectively (Tian et al., 2023). According to results depicted in Fig. S3A, the AM content was calculated in Table S2. HAMS showed the highest AM content (66.6%), followed by NMS (29.1%) and WMS (9.8%). For debranched starch, SEC chromatograms (Fig. S3B) can be divided into three regions: AP_S($R_h \leq 2$ nm), AP_L ($2 < R_h \leq 5$ nm) and AM ($R_h > 5$ nm) (Zhong, Herburger, et al., 2022). WMS had lowest AM content (4.2%), but had highest AP_S content (81.2%). HAMS starch had the highest AM content (33.7%) and average chain length of AM (940.2 DP). In the present research, the results were in line with previous research on WMS, NMS and HAMS (Tian et al., 2022; Tian et al., 2023; Zhong, Herburger, et al., 2022; Zhong, Tian, et al., 2021).

3.2. Starch granular shape and gelation observation

NMS analysed by polarized microscopy (Fig. 1) and light microscopy (Fig. S4) showed that the birefringence (maltese cross) effect, which reflects the anisotropic (radial) organization of the glucan chains, started to decrease from 0 min to 2.5 min (68 °C), and disappeared at 3.5 min (80 °C), underlining the loss of granular structure ordering at 3.5 min (80 °C) during the heating stage. WMS showed a faster disappearence of the maltese cross from 0 min to 2 min (61 °C), and disappeared at 3 min (73 °C). As compared to WMS and NMS, HAMS starch granules showed a clear maltese cross from 0 min to 4 min (85 °C), and its intensity started to fade towards 9 min (75 °C), until it disappeared.

Scanning Electron Microscopy (SEM) images of the WMS freeze-dried samples (Fig. 2) indicated that starch granules started to swell at 2.5 min (68 °C). When starch was heated for 3 min (73 °C), a loose gelation network structure formed, with several enlarged starch granules embedded in the gelation network structure. With continued heating, enlarged starch granules started to disrupt and the gelation network gradually turned into a flaky structure at 3.5 min (80 °C). When heating for 9 min (75 °C), the flaky structure became denser and the pores smaller. When heating for 13 min (50 °C), the flaky structure gradually merged into a dense gel. After grinding the freeze-dried starch gel obtained after 3 min (73 °C) into fine particles (Fig. S5), it became apparent that all the starch granules gelatinized. These fragments continue to shatter, forming smaller fragments until they are completely gelatinized at 4 min (85 °C), which coincided with the peak viscosity.

Scanning Electron Microscopy (SEM) images of the NMS freeze-dried samples (Fig. 3) revealed that the granules became larger and irregular at 2.5 min (68 °C), which is an effect of swelling. Importantly, pores were generated on the granular surface at this stage (Fig. 3), and this was accompanied by leaching of inner blocklets from the swelling granular

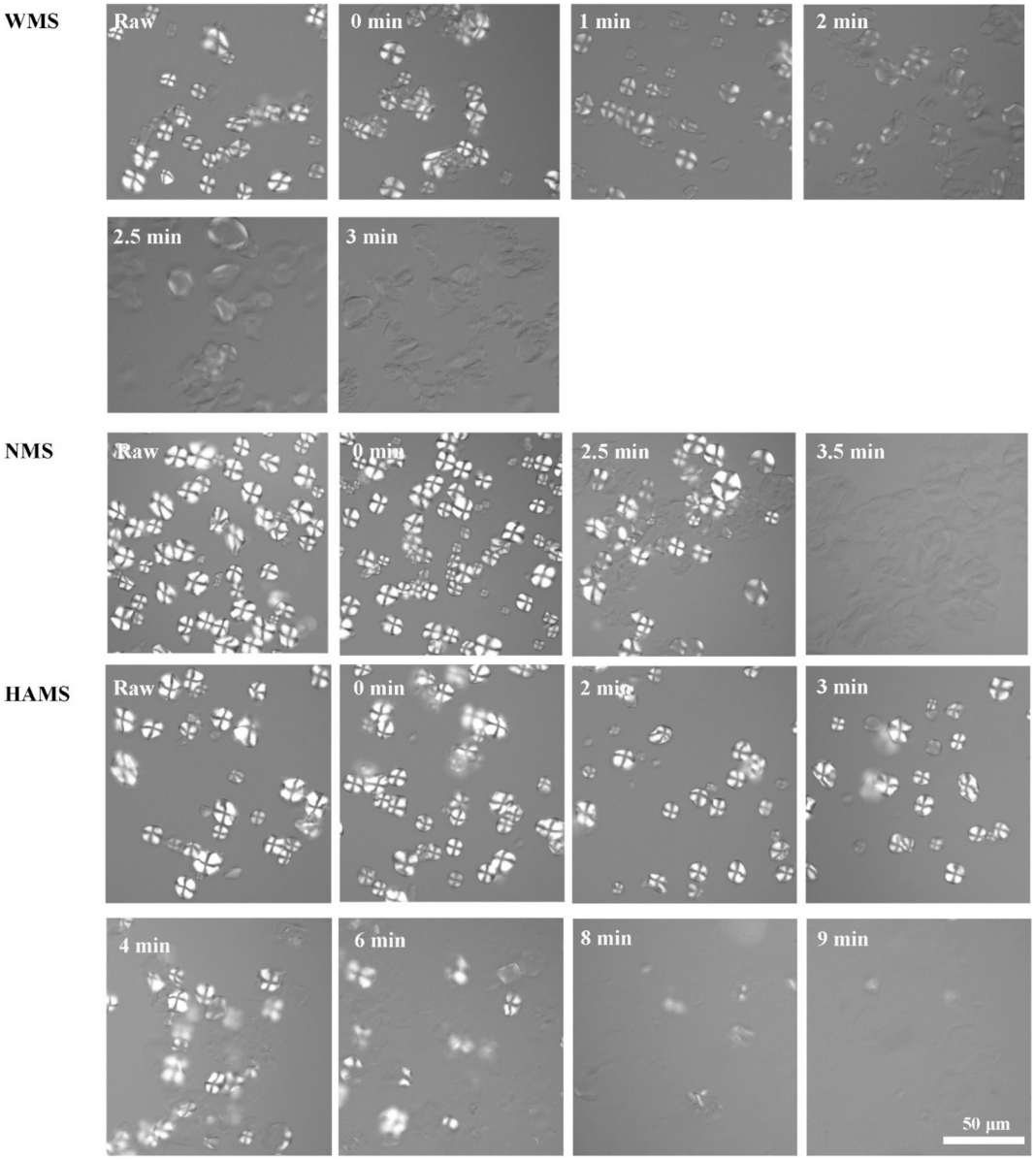

Fig. 1. Microphotographs of WMS, NMS and HAMS granules during the RVA process as monitored by polarizing light. Scale bar = 50 μm.

matrix (Ma et al., 2022), which were found to be important for the upcoming gelation of starch. The granules were elongated further and outer shells from disrupted granules were observed at 3.5 min (80 °C). At 4.5 min (92 °C holding), numerous blocklets had leached out, melted, and reorganized into a loose gelation network structure where fully swelled starch granules constituted the network nucleus. At the point of peak viscosity (5.5 min, 95 °C), a dense matrix structure composed of leached starch molecules with some apparent large pores but lacking intact starch granules was observed. However, after grinding the 5 min freeze-dried starch gel into fine particles, some granules were identified (Fig. S6), suggesting that remaining compact granules were still in the nucleus constituting the gel network structure with the high viscosity, which is in agreement with earlier reports (Balet et al., 2019; Batey, 2007). These granules were destroyed within the next 0.5 min (6 min, 95 °C) at the same temperature interval, and the gel structure rapidly evolved into a loosely packed, flaky structure with smaller pores. As AP is the main component of NMS (Zhong et al., 2020), the present data suggest that AP mainly contributed as a backbone to the gel structure, while AM filled in this gel network. It is worth noting that the viscosity decreased at this point, implying that the gel network structure lacked starch granules present; compared to gel networks containing starch granules, the granule-free network had a lower resistance to deformation. During the cooling stage (9 min, 75 °C) and final holding stage (13 min, 50 °C), the flaky structure became denser, more homogeneous and the pore size further decreased, suggesting a gelation self-assembly process of the starch molecules, especially AM molecules, towards a more ordered structure with decreasing temperatures (Li, Gidley, & Dhital, 2019; Zhong, Tai, et al., 2022).

Interestingly, during the decreasing temperature ramp from 95 °C to 50 °C (6 → 13 min), typically characteristic of a decrease in viscosity (granular disintegration) and a following increase of viscosity (gelation) was observed (Fig. 1), resulting in the flaky structure to become increasingly ordered. The decreased viscosity from 6 min to 9 min is merely attributed to granular disintegration and our data suggested that this effect can be related to the presence of swollen starch granules in a paste network structure. The disintegration of starch granules at 5 min induced an unstable paste structure, which became gradually weaker under a relative high temperature range (95 °C → 75 °C). In the final holding stage, due to the further decreased temperature (75 °C → 50 °C), the gel network appeared to become thermally disrupted, and the

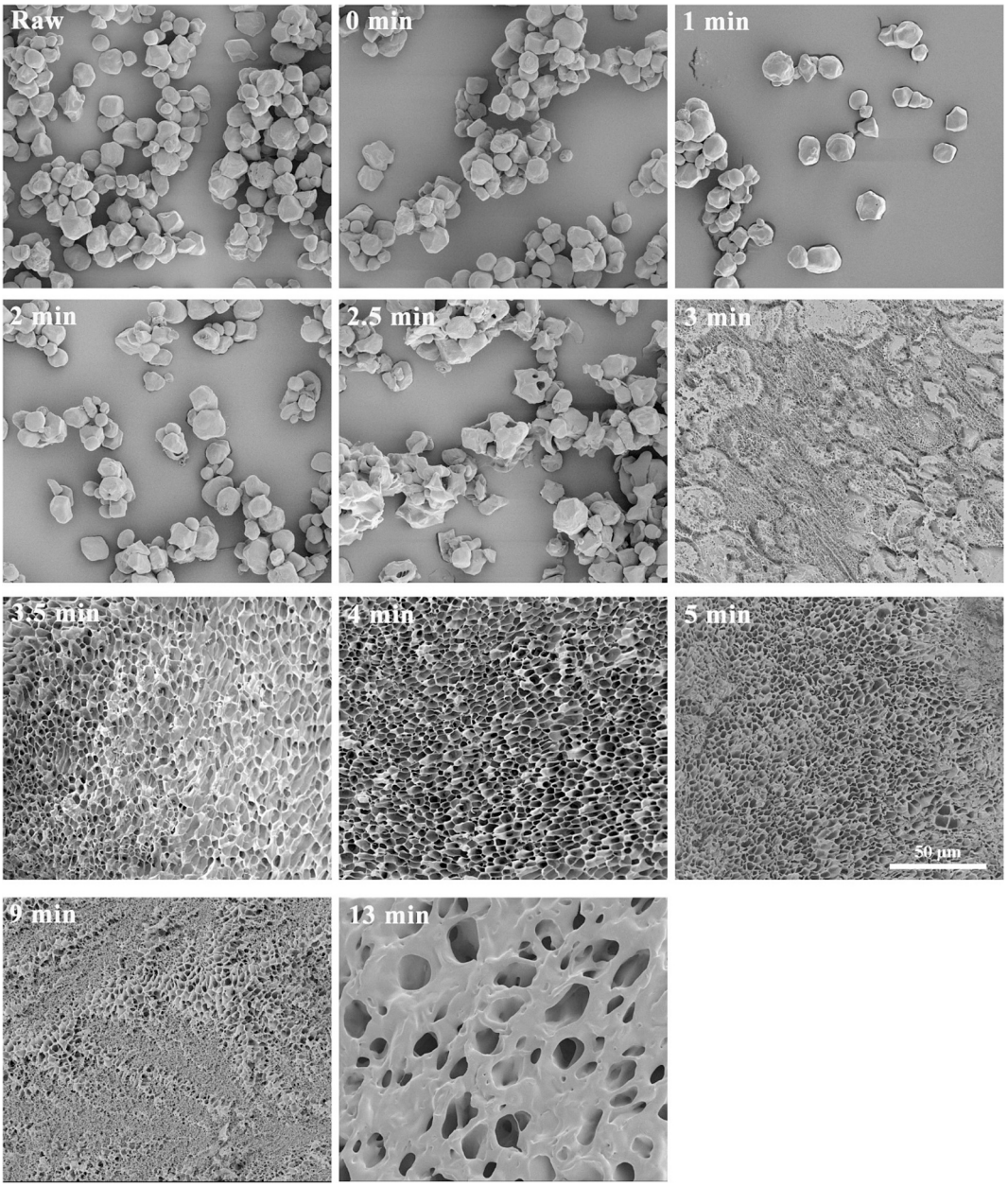

Fig. 2. Morphology of WMS starch granules during RVA process as imaged by SEM. Scale bar = 50 μm.

realignment of mainly AM molecules at 50 °C (Li et al., 2019; Zhong, Tai, et al., 2022) resulted in increased viscosity. The performance of HAMS differed strongly from WMS and NMS. HAMS granules exhibited an intact morphological structure during the first 3 min, and starch granules started to swell and pores appeared on the surface, releasing blocklets at 4 min. From 6 min to 8 min, blocklets continued to form, leading to the formation of a gel network(Fig. 4). The storage and loss moduli are crucial rheological parameters that signify the elastic strength of gels and the viscous behaviour of a starch paste, respectively (Ding et al., 2024). The rheological properties of starch gels at 1 Hz (Table S1) showed that HAMS had higher storage modulus than WMS and NMS, generating a stronger elastic gel network structure as expected for high amylose content gels (Ai & Jane, 2015).

Besides, the gelatinization peak temperatures found in this study showed inconsistency between the RVA and DSC results (Fig. S2 and Table S1). In previous studies, NMS starch (S4126, Sigma-Aldrich) showed a peak temperature of 91 °C in RVA but only 79 °C in DSC, which is consistent with the results of this study (Wang, Guo, Fan, Feng, & Wei, 2018). Other studies have also reported a peak gelatinization temperature of 83.1 °C (Chen et al., 2018) and 76.37 °C (Zou, Xu, Tang, Wen, & Yang, 2020) in RVA for commercial NMS starch. The gelatinization temperature of starch can be affected by genotype background of the plant, the growth environment, and the extraction method (Abegunde, Mu, Chen, & Deng, 2013; Xu et al., 2024). In this study, the pasting temperature in RVA represents the temperature at which the maximum viscosity is reached, while in DSC it represents the temperature at which the maximum rate of starch gelatinization occurs. Hence, the two methods used represent different mechanisms and therefore differences were expected.

Interestingly, HAMS showed weak pasting parameters when compared with NMS and WMS starch. During the RVA process, HAMS starch always maintained its particle structure, while no visible breakdown products appeared. This can be attributed to the fact that the RVA system used in the present study applies a maximum temperature of 95 °C, which is insufficient to completely gelatinize high-amylose starch and resulted in the weak pasting parameters. Previous research using the

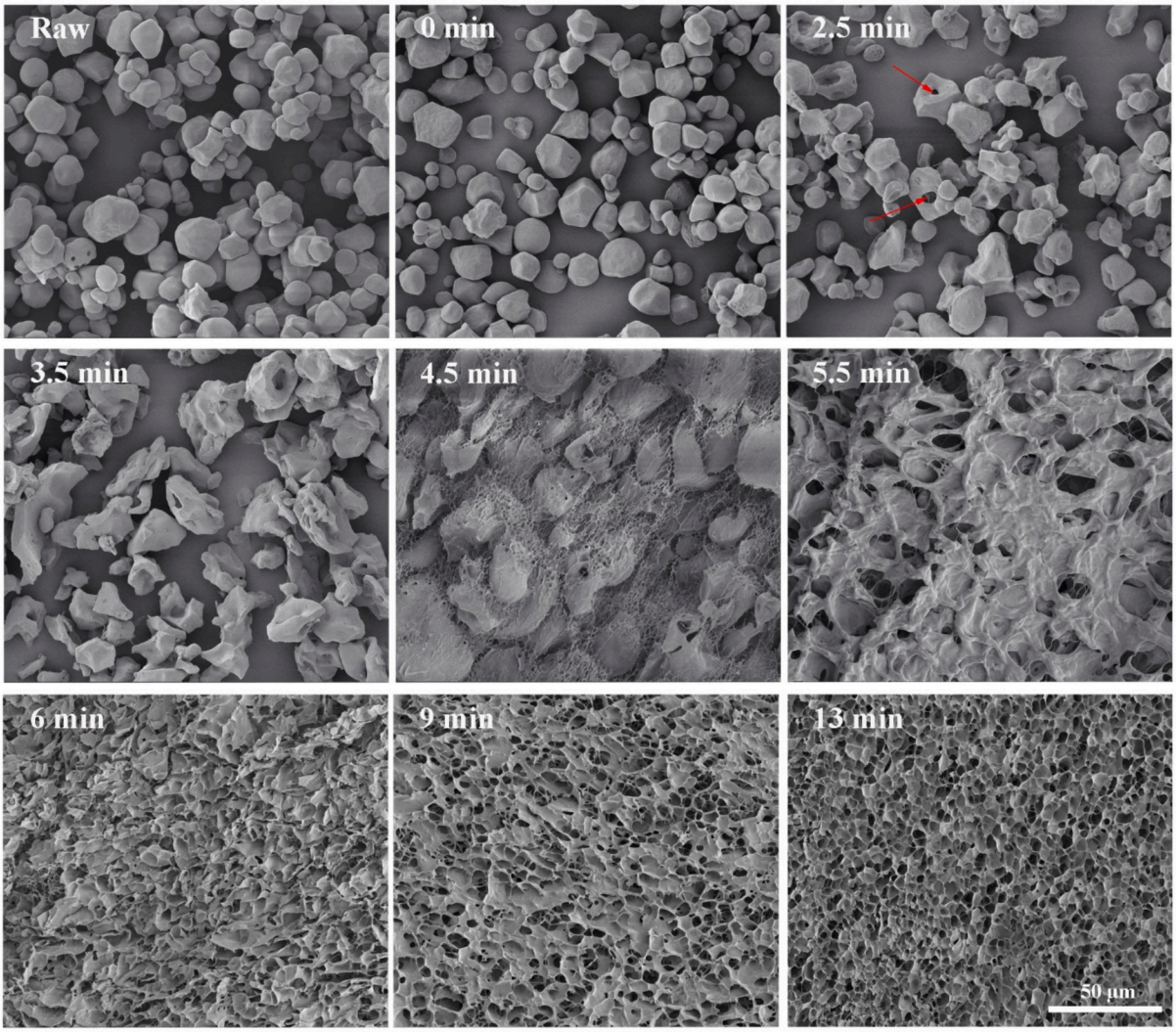

Fig. 3. Morphology of NMS starch granules during RVA process analysed by SEM. Scale bar = 50 μm.

RVA4800 system, which allow for heating up to 140 °C, showed that such higher temperatures achieved complete gelatinization of high-amylose starch (Tian et al., 2022). Finally, SEM analysis of the ground sample showed that the HAMS starch grains swelled during the gelatinization, but did not break down completely (Fig. S7).

3.3. Crystalline and nano-lamellar structure of starch

WAXS analysis (Fig. 5A) revealed that the crystalline polymorph of WMS and NMS showed strong peaks at 15°, 17°, 18° and 23°, which is typical for the A-type starch. During RVA process, WMS remained unchanged at 50 °C, demonstrating that the high-speed stirring during the 50 °C incubation had no effect on the crystalline structure of WMS granules. The peak intensity of all peaks kept decreasing slowly within the next 2 min (50 → 68 °C) period and dropped significantly from 2.5 min to 3 min (68 → 73 °C), indicating that the entire crystalline structure was fully disrupted at 68 °C. Within the next 1 min (73 → 85 °C), the crystallinity disappeared, showing that the crystalline structure was lost when the viscosity reached its maximum (peak viscosity). In the cooling and holding stages, no crystalline structure was detected, demonstrating that no starch crystals formed within this short-term gelation. Moreover, the analysis of gel samples by WAXS showed that no helical or crystal structure formed due to the retrogradation of AM molecules in the final holding stage. Thus, the effect of AM molecules on increasing viscosity was likely attributed to entanglement of flexible AM molecules with AP, increasing the stability of the gel network. Similar results were found for NMS (Fig. 5B), from 0 to 2.5 min (50 → 68 °C), the peak intensity of 17°a nd 18° decreased slowly, while during the next 1 min (68 → 80 °C), the crystalline disrupted completely. HAMS samples contained typical B-type starch with a strong peak at 5.6°, 17°, 22° and 24°, which is in line with a previous report (Zhong, Tian, et al., 2021). As the gelatinization reaction progressed, the peak intensity of HAMS starch gradually decreased until 8 min (86 °C). After 8 min, the peak intensity of HAMS increased slightly, which may be caused by the amylose forming a gel network and by recrystallization. In contrast to WMS and NMS, the WAXS patterns of HAMS starch suggest a persistent crystal structure lacking an amorphous state. This might by caused by an incomplete gelatinization of HAMS.

Similar to WAXS, SAXS analysis of WMS and NMS during the RVA imposed gelation process (Fig. 5B, D) showed that the lamellar structure of WMS and NMS disappeared in the heating stage from 2.5 min to 3 min (68 → 73 °C) and from 2.5 min to 3.5 min (68 → 80 °C). This is the point at which the viscosity started to rise, suggesting that the crystalline structure and lamellar structure were disrupted simultaneously, which then increased the viscosity. During the following process, no nano-range structures were formed. This is in agreement with microscopy data as outlined above. Different from WMS and NMS, the lamellar structure of HAMS starch disappeared from 3 min to 4 min (73 → 85 °C). Combined with WAXS result, the lamellar structure of HAMS disappeared from 3 to 4 min, which increased the viscosity, but due to

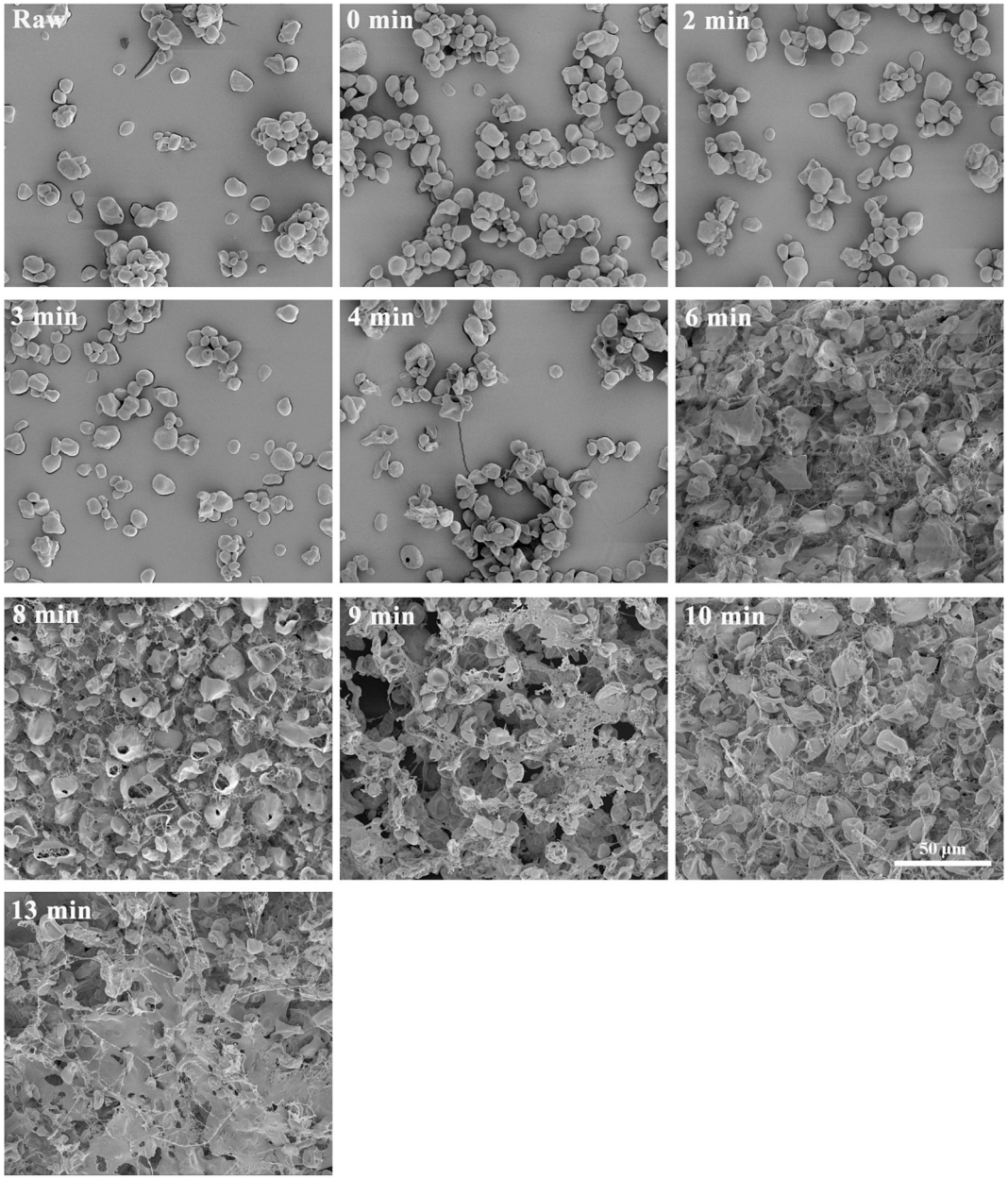

Fig. 4. Morphology of HAMS granules during RVA process under SEM. Scale bar = 50 μm.

incomplete gelatinization, some crystal structures remained, explaining the lower viscosity observed.

3.4. Additional structural properties of starch during RVA process

The data so far account for the morphological parameters (as studied by light and polarized microscopy and SEM) and the crystalline structure of the starch (WAXS and SAXS). The data showed that WMS, NMS and HAMS have the same trend, to gain deeper insights into starch structural remodelling during the RVA process, NMS starch was chosen to analyse the short-range ordered structure (FTIR), helical structure (SS-NMR), granule size and surface structure at high resolution (AFM analysis).

3.4.1. Short-range ordered structure

ATR-FTIR analysis provides flexibility to analyse starch samples in a range of physical forms, particularly in their differential hydrated state, enabling to observe spectral differences as an effect of the level of hydration (Warren, Gidley, & Flanagan, 2016). ATR-FTIR spectroscopic analysis also provides insights into the structural ordering of the granular surface by three peaks at 1047 cm^{-1}, 1022 cm^{-1}, and 995 cm^{-1} (Warren et al., 2016). For native starch, similar FTIR spectra after deconvolution were also reported for NMS purchased from Sigma-Aldrich (Wang et al., 2018; Zhang et al., 2017). For the RVA process of NMS, the peak at 1047 cm^{-1} disappeared at 2.5 min (68 °C), the intensity of peak at 1022 cm^{-1} and 995 cm^{-1} increased throughout the entire RVA process, especially after 5.5 min (95 °C) (Fig. 6A). The peaks at the above mentioned wavelengths identify the crystalline state, amorphous state, and hydration of starch granular surface (Kizil, Irudayaraj, & Seetharaman, 2002; Warren et al., 2016). The ordered degree and the relative proportion of dynamic/amorphous to stiff/ordered carbohydrate structures have been empirically suggested to be quantified by the absorbance ratios at wavelengths of 1045/1022 cm^{-1} and 1022/995 cm^{-1}, respectively (Sevenou, Hill, Farhat, & Mitchell, 2002). The present data indicate that the granular surface structure ordering was lost at 2.5 min (68 °C), prior to the loss of crystalline and lamellar

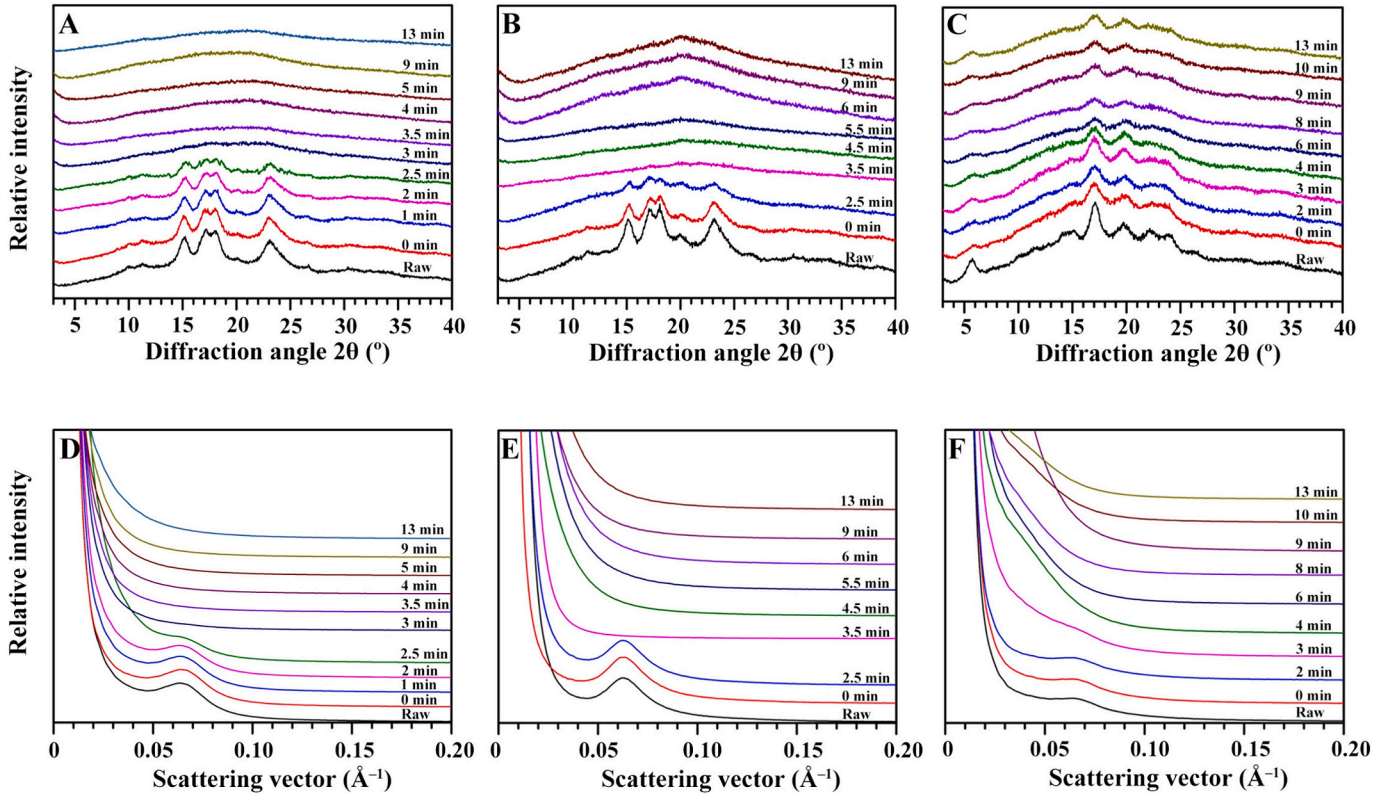

Fig. 5. WAXS and SAXS profiles of starch granules during RVA process. (A): WAXS of WMS; (B): WAXS of NMS; (C): WAXS of HAMS; (D): SAXS of WMS; (E): SAXS of NMS; (F): SAXS of HAMS.

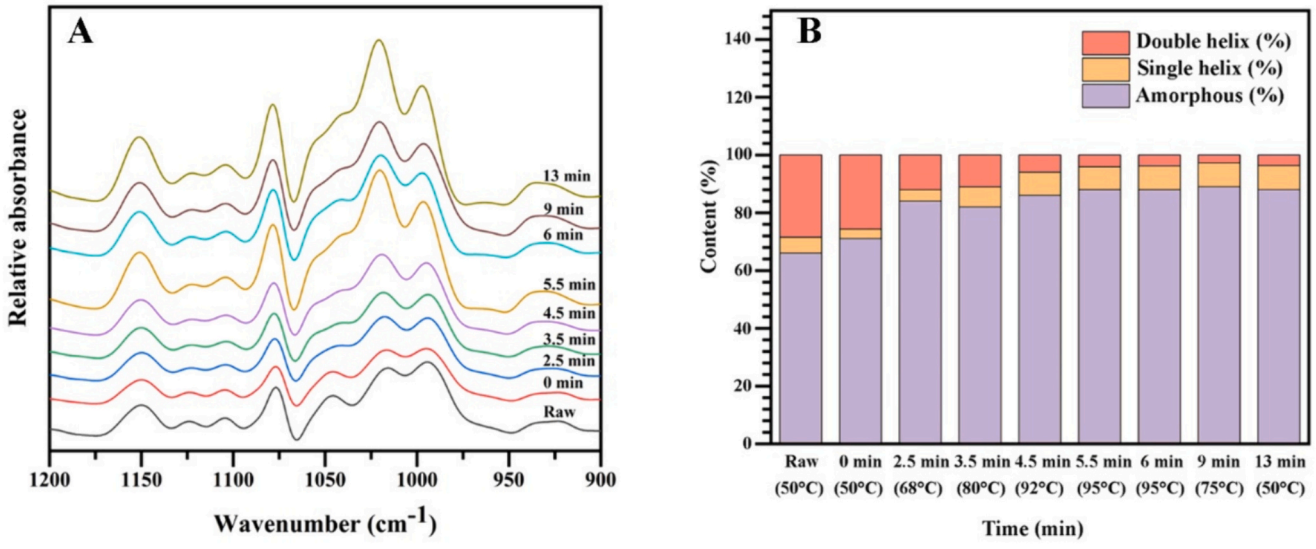

Fig. 6. ATR-FTIR spectrum (A) and ^{13}C NMR (B) of NMS starch granules during the RVA process.

structure ordering of the whole granule (Fig. 5). This implies that the loss of structural ordering of NMS during the RVA process was initiated from the granular surface and extended to the granular internal regions. The intensities of peaks at 1022 cm^{-1} and 995 cm^{-1} increased significantly from 4.5 min to 6 min (92–95 °C), then decreased from 6 min to 9 min (95–75 °C), and increased again from 9 min to 13 min (75–50 °C), which is in agreement with the changes in viscosity. Hence, these data suggest that the viscosity of the starch paste was related to the hydration level of the paste, and the amorphous state of granular surface contributed to the high hydration level.

3.4.2. *Helical structure*

The helical structure of the NMS during the RVA processing, assessed via solid state-NMR (SS-NMR) (Fig. 6B), revealed that the relative proportions of both double- and single helix contents surprisingly started to decrease already in raw starch at 0 min, indicating that the high-speed short-time stirring at 50 °C partly disrupted the packing of helical structures at the initial stage of the RVA (Fonseca, Halal, Dias, & Zavareze, 2021). The relative amount of double helices decreased most rapidly at 2.5 min within the first 2.5 min (50 → 68 °C), reaching 13%, suggesting hydrothermal unpacking of a larger fraction of double helical

structures of the starch granules. Interestingly, during the following 1 min (68 → 80 °C) the relative amount of double helical content remained unchanged, while the amount of single helices increased 3%, suggesting reorganization of AM molecules into single helical structures during the heating stage. In the following 4.5 min, the double helical structures were further unwound, while the single helices remained unchanged. This may be attributed to the low thermal stability of double helices, and the high thermal stability of re-formed single helices in the NMS gel. The relative amounts of both single and double helices increased slightly in the final holding stage (13 min, 50 °C).

3.4.3. Granule and agglomerate size distribution of starch

Granule and agglomerate size distribution data (Table 1) showed that the average size of the starch granules (D[4,3], the volume-weighted mean diameter) was unchanged at 0 min, demonstrating insignificant swelling of the starch granules at 50 °C. The granular size significantly increased within the next 4.5 min, due to the rapid swelling of starch granules under high temperatures (95 °C). Larger particles (>100 μm), also considered as agglomerate granules appeared from 5.5 min (95 °C holding), which is also the point of peak viscosity, and this also corresponds to previous reports that when starch granules swell to their maximum volume, the viscosity also can obtain the highest value (Wang et al., 2021). Furthermore, starch granules kept increasing during the next 7.5 min due to the fragments formed following granular fragmentation, which aggregated to form a compound structures leading to a rapid increase in volume when measuring granule size distribution (Fig. S6).

3.4.4. AFM analysis of starch

Atomic Force Microscopy (AFM) is a super-high-resolution microscopy technique enabling the observation of surface morphology and properties of specimens at the sub-nanoscale (Chen et al., 2021). Although, the surfaces of the starch granules appeared relatively smooth when observed using light or electron microscopy (Figs. 1 & 3), they appeared relatively rough when observed at the nanoscale using AFM (Fig. S8), which agreed with previous AFM data (Peroni-Okita et al., 2015). The AFM images (Fig. S8) revealed increased size of blocklets at 2.5 min (68 °C) of the RVA heating phase, indicating that the swelling of starch granules was due to swelling of individual blocklets, which is in agreement with the disordering of granular surface structure as analysed by FTIR. However, most blocklets were hydrated and merged within the next 1 min (68–80 °C). As shown in the 3D diagram, at 3.5 min (Fig. S8), numerous protuberances appear on the surface of the starch granules, due to the rapid expansion stage. In the full gelation stage (6 min, 95 °C holding), a homogenous surface of the gel structure with many small bulges was evident.

Table 1
Granule and agglomerate size distribution of NMS starch during RVA process[a].a, b

	Granule size distribution		
	D [3,2] (μm) [b]	D [4,3] (μm) [b]	d (0.5) (μm) [b]
Raw	8.3 ± 0.3a	15.3 ± 0.1a	15.2 ± 0.1a
0 min	8.9 ± 0.1a	15.6 ± 0.2a	15.5 ± 0.2a
2.5 min	15.9 ± 0.2b	28.1 ± 0.7ab	26.9 ± 0.5a
3.5 min	23.1 ± 0.4c	40.9 ± 1.0abc	33.0 ± 0.3a
4.5 min	21.4 ± 0.4c	48.8 ± 0.0bc	38.8 ± 0.8a
5.5 min	23.9 ± 0.3c	57.5 ± 5.2c	36.2 ± 0.5a
6 min	15.6 ± 0.7b	89.2 ± 0.7d	30.6 ± 2.9a
9 min	35.7 ± 0.9d	339.4 ± 28.4e	94.3 ± 14.7b
13 min	56.8 ± 5.3e	719.3 ± 27.4f	480.6 ± 51.7c

[a] Data are means ± standard deviations ($n = 3$). Values in the same column with different letters are significantly different ($p < 0.05$).

[b] D[3,2], surface-weighted mean diameter; D[4,3], volume-weighted mean diameter; The d(0.5) is the granule size at which 50% of all the granules by volume are smaller.

3.5. Structural evolution of starch during RVA process

This study reports on the structural evolution of WMS, NMS and HAMS during a standardised RVA mediated gelatinization-gelation process. According to the classification of five main stages of RVA (Balet et al., 2019), the starch structural changes at the different stages were investigated. For NMS and WMS (Fig. 7), at the initial stage (stage 1), the helical- and crystalline structures were partly disrupted. At the heating stage (stage 2), the helical structures were abolished, the inner blocklets and starch granules swelled and pores were generated, thereby inducing the leaching of inner blocklets. The nano-lamellar and crystalline structures, and birefringence were disrupted simultaneously, and inner blocklets swelled and leached starch molecules formed a loose gel network structure around the remaining swelling starch granules. At the holding stage (stage 3), starch granules were mostly disrupted, and remaining starch granules localised in the nucleus, constituting the dense, homogenous, and thermally stable gel structure with leached starch molecules. Upon reaching peak viscosity, all starch granules were disintegrated, and a disordered flaky gel structure emerged. In the later cooling (stage 4) and final holding stages (stage 5), the flaky gel structure became more ordered and exhibited smaller pore sizes.

Taken together, the present study showed that the WMS and NMS gels with peak viscosity entered a state where most granules were disrupted, while only few granules remained, all of which leading to a gel structure in which the remaining granules constituted the core and the leached starch molecules acted as fillers. The following decrease in viscosity after peak viscosity may have been due to the complete loss of granular structures in the gel network, thereby weakening the stability of the gel. The final increase in viscosity at the final holding stage was attributed to the reorganization of starch molecules in which amylose molecules are dominant, this was suggested by the obervation that NMS had a higher setback viscosity than WMS.

However, HAMS displayed a very low peak viscosity when heated at 95 °C, which is due to the high gelatinization point for this high amylose starch (Tian et al., 2022). Consequently, this system provided little information in terms of structural changes during heating and cooling processing. Nevertheless, the trend of multi-scale structural changes found for HAMS was consistent with the more detailed data obtained for NMS and WMS, i.e. a disappearence of helical and crystal structures during the heating stage, followed by the transformation of the gel network into a flaky gel structure in the cooling stage, which then became more ordered in the final holding stage. However, due to the high gelatinization temperature of HAMS, these trends were incomplete, for example, the crystal structure was not completely disrupted, and the gel network structure also contained many ungelatinized starch granules. Previous studies have also reported that during gelatinization, the granular structure of starch persists even after the loss of birefringence. (Cai et al., 2014; Guo, Zhang, Bian, Cao, & Wei, 2020). For HAMS, a high-temperature protocol such as the RVA4800 instrument will provide additional information at the high-pressure state (Ren et al., 2023; Tian et al., 2022). However, for comparative reasons, the standard RVA protocol was chosen in this research. Most laboratories currently still use regular ambient-pressure RVA as the standardised method for monitoring high amylose pasting (Liu et al., 2024; No & Shin, 2023; Xu et al., 2024), and the data in this study can provide reference for these studies. It should be noted that, for other starches like potato, rice and cassava starch, similar trends can be observed, but due to the different species types, there may be some differences in the specific viscosity values and gelatinization time points preventing clear comparative interpretation of the data. Hence a more isogenic starch system was analysed in our study.

4. Conclusion

This study has systematically pioneered the multi-scale granular and structural changes during pasting and subsequent gel formation by

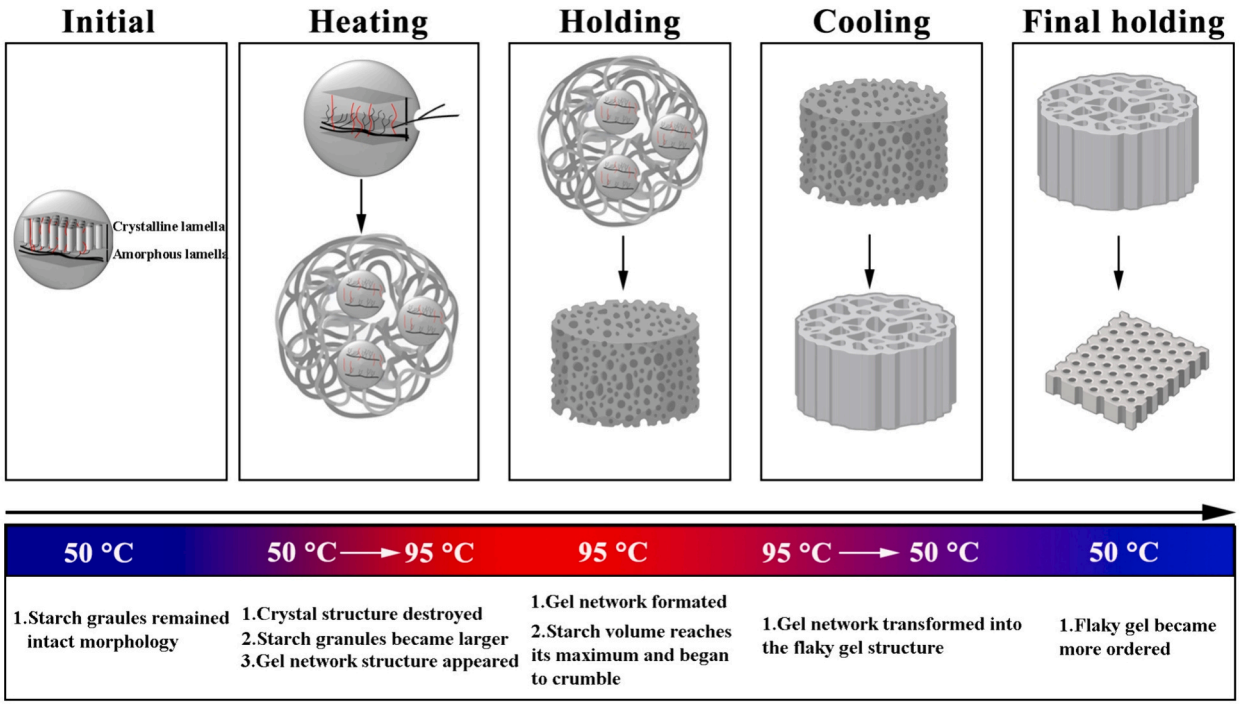

Fig. 7. Schematic diagram of the changes in the multi-scale structure of starch during the RVA process.

WMS, NMS and HAMS. These processes were analysed using a RVA-mediated process widely used in industry. Initially, the starch granules maintained their intact granular structure and even their birefringence at 50 °C. Subsequently, during the heating stage, the helical and crystal structure of starch disappeared and a gel network structure began to form. During the holding phase, the starch granules reached their maximum size and then split into fragments. However, for the HAMS sample, partially ungelatinized starch granules were found, as an effect of insufficient gelatinization. The data in the present study strongly expand our understanding of the dynamic molecular rearrangements occurring during starch pasting followed by subsequent gelation and initial retrogradation. These insights are key for understanding starch as thickener in the food, material and hydrocolloids industry. However, due to the structural diversity of starches from different botanical sources and genotypes, like potato, rice, cassava starch, there may be some differences in structural changes, such as the specific viscosity values and gelation time points preventing clear comparative interpretation of the data, so further investigation needs to be operated on starches from different botanical sources and genotypes. Moreover, understanding how the fine structure of amylopectin affects starch viscosity still requires further investigations.

CRediT authorship contribution statement

Ke Guo: Writing – review & editing, Writing – original draft, Investigation, Formal analysis, Data curation. **Yu Tian:** Investigation, Data curation. **Dagmara Podzimska-Sroka:** Writing – original draft. **Jacob Judas Kain Kirkensgaard:** Writing – review & editing, Methodology, Investigation. **Klaus Herburger:** Writing – review & editing. **Kasper Enemark-Rasmussen:** Investigation. **Tue Hassenkam:** Methodology, Investigation. **Bent Larsen Petersen:** Writing – review & editing, Investigation. **Andreas Blennow:** Writing – review & editing, Supervision, Methodology, Funding acquisition. **Yuyue Zhong:** Writing – review & editing, Supervision, Investigation.

Declaration of competing interest

The authors declare no conflict of interest.

Data availability

Data will be made available on request.

Acknowledgments

This study was financially supported by grants from “HIAMBA - grain, flour, bread & bakery products preventing type 2 diabetes” Innovation Fund Denmark (Project 9067-00004 A), Jiangsu Funding Program for Excellent Postdoctoral Talent. Data were generated by accessing research infrastructure at University of Copenhagen, including FOODHAY (Food and Health Open Innovation Laboratory, Danish Roadmap for Research Infrastructure). And we thanks for Li Ding, from Copenhagen University for the help of measuring rheological properties.

Appendix A. Supplementary data

Supplementary data to this article can be found online at https://doi.org/10.1016/j.foodchem.2024.140817.

References

Abegunde, O. K., Mu, T.-H., Chen, J.-W., & Deng, F.-M. (2013). Physicochemical characterization of sweet potato starches popularly used in Chinese starch industry. *Food Hydrocolloids, 33*(2), 169–177.

Ai, Y., & Jane, J. (2015). Gelatinization and rheological properties of starch. *Starch, 67*, 213–224.

Balet, S., Guelpa, A., Fox, G., & Manley, M. (2019). Rapid Visco Analyser (RVA) as a tool for measuring starch-related physiochemical properties in cereals: A review. *Food Analytical Methods, 12*, 2344–2360.

Batey, I. (2007). Interpretation of RVA curves. *The RVA handbook*, 19–30.

Cai, C., Cai, J., Man, J., Yang, Y., Wang, Z., & Wei, C. (2014). Allomorph distribution and granule structure of lotus rhizome C-type starch during gelatinization. *Food Chemistry, 142*, 408–415.

Castanha, N., Rojas, M. L., & Augusto, P. E. (2021). An insight into the pasting properties and gel strength of starches from different sources: Effect of starch concentration. *Scientia Agropecuaria, 24*, 203–212.

Chen, L., McClements, D. J., Ma, Y., Yang, T., Ren, F., Tian, Y., & Jin, Z. (2021). Analysis of porous structure of potato starch granules by low-field NMR cryoporometry and AFM. *International Journal of Biological Macromolecules, 173*, 307–314.
Chen, L., Tian, Y., Bai, Y., Wang, J., Jiao, A., & Jin, Z. (2018). Effect of frying on the pasting and rheological properties of normal maize starch. *Food Hydrocolloids, 77*, 85–95.
Chen, P., Yu, L., Simon, G. P., Liu, X., Dean, K., & Chen, L. (2011). Internal structures and phase-transitions of starch granules during gelatinization. *Carbohydrate Polymers, 83*, 1975–1983.
Cozzolino, D. (2016). The use of the rapid visco analyser (RVA) in breeding and selection of cereals. *Journal of Cereal Science, 70*, 282–290.
Ding, L., Blennow, A., & Zhong, Y. (2024). *Differential roles of C-3 and C-6 phosphate monoesters in affecting potato starch properties*. Grain & Oil Science and Technology.
Fonseca, L. M., Halal, S. L., Dias, A. R., & Zavareze, E. D. (2021). Physical modification of starch by heat-moisture treatment and annealing and their applications: A review. *Carbohydrate Polymers, 274*, Article 118665.
Guo, K., Liu, T., Xu, A., Zhang, L., Bian, X., & Wei, C. (2019). Structural and functional properties of starches from root tubers of white, yellow, and purple sweet potatoes. *Food Hydrocolloids, 89*, 829–836.
Guo, K., Zhang, L., Bian, X., Cao, Q., & Wei, C. (2020). A-, B- and C-type starch granules coexist in root tuber of sweet potato. *Food Hydrocolloids, 98*, Article 105279.
Kizil, R., Irudayaraj, J., & Seetharaman, K. (2002). Characterization of irradiated starches by using FT-Raman and FTIR spectroscopy. *Journal of Agricultural and Food Chemistry, 50*, 3912–3918.
Li, H., Gidley, M. J., & Dhital, S. (2019). High-amylose starches to bridge the "Fiber gap": Development, structure, and nutritional functionality. *Comprehensive Reviews in Food Science and Food Safety, 18*, 362–379.
Li, H., Prakash, S., Nicholson, T. M., Fitzgerald, M. A., & Gilbert, R. G. (2016). The importance of amylose and amylopectin fine structure for textural properties of cooked rice grains. *Food Chemistry, 196*, 702–711.
Liu, S., Yuan, T. Z., Wang, X., Reimer, M., Isaak, C., & Ai, Y. (2019). Behaviors of starches evaluated at high heating temperatures using a new model of rapid Visco analyzer – RVA 4800. *Food Hydrocolloids, 94*, 217–228.
Liu, Z., Chen, L., Bie, P., Xie, F., & Zheng, B. (2021). An insight into the structural evolution of waxy maize starch chains during growth based on nonlinear rheology. *Food Hydrocolloids, 116*, Article 106655.
Liu, Z., Cheng, G., Gu, Z., Zhou, Q., Yang, Y., Zhang, Z., Zhao, R., Li, C., Tian, J., Feng, J., & Jiang, H. (2024). Dynamic rheological behavior of high-amylose wheat dough during various heating stages: Insight from its starch characteristics. *International Journal of Biological Macromolecules, 132111*.
Lu, D., Wang, D., Zhao, J., & Lu, W. (2008). Effects of reaction program and starch concentration on rapid viscosity analysis (RVA) profiles of waxy and Normal corn starches. *Food Science, 25*, 35–39.
Ma, M., Xu, Z., Chen, X., Zhang, C., Liu, Z., Cantre, D., Li, H., Sui, Z., & Corke, H. (2022). Architecture of outer shell and inner blocklets of rice starch granule is related to starch granule-associated proteins. *Food Hydrocolloids, 127*, Article 107551.
Mahmood, K., Kamilah, H., Shang, P. L., Sulaiman, S., & Ariffin, F. (2017). A review: Interaction of starch/non-starch hydrocolloid blending and the recent food applications. *Food Bioscience, 19*, 110–120.
No, J., & Shin, M. (2023). Structures and digestibility of B-type high-amylose rice starches compared with A-type high-amylose rice starches. *Journal of Cereal Science, 103713*.
Peroni-Okita, F. H., Gunning, A. P., Kirby, A. R., Simão, R. A., Soares, C. A., & Cordenunsi, B. R. (2015). Visualization of internal structure of banana starch granule through AFM. *Carbohydrate Polymers, 128*, 32–40.
Ren, Y., Liang, W., Zhong, Y., Hebelstrup, K. H., Blennow, A., & Ai, Y. (2023). Impact of a full range of amylose level on pasting and gelling properties of barley starches at high-temperature heating. *Starch, 2200167*.
Ridout, M., Gunning, A., Parker, M., Wilson, R., & Morris, V. (2002). Using AFM to image the internal structure of starch granules. *Carbohydrate Polymers, 50*, 123–132.
Sevenou, O., Hill, S. E., Farhat, I. A., & Mitchell, J. R. (2002). Organisation of the external region of the starch granule as determined by infrared spectroscopy. *International Journal of Biological Macromolecules, 31*, 79–85.
Shivaraju, V. K., Appukuttan, S. V., & Kumar, S. (2018). The influence of bound water on the FTIR characteristics of starch and starch nanocrystals obtained from selected natural sources. *Starch, 71*, 1700026.
Tan, I., Flanagan, B. M., Halley, P. J., Whittaker, A. K., & Gidley, M. J. (2007). A method for estimating the nature and relative proportions of amorphous, single, and double-helical components in starch granules by ^{13}C CP/MAS NMR. *Biomacromolecules, 8*(3), 885–891.
Tao, K., Li, C., Yu, W., Gilbert, R. G., & Li, E. (2019). How amylose molecular fine structure of rice starch affects functional properties. *Carbohydrate Polymers, 204*, 24–31.
Tian, Y., Qu, J., Zhou, Q., Ding, L., Cui, Y., Blennow, A., Zhong, Y., & Liu, X. (2022). High pressure/temperature pasting and gelling of starch related to multilevel structure-analyzed with RVA 4800. *Carbohydrate Polymers, 295*, Article 119858.
Tian, Y., Wang, Y., Herbuger, K., Petersen, B. L., Cui, Y., Blennow, A., … Zhong, Y. (2023). High-pressure pasting performance and multilevel structures of short-term microwave-treated high-amylose maize starch. *Carbohydrate Polymers, 322*, Article 121366.
Wang, J., Guo, K., Fan, X., Feng, G., & Wei, C. (2018). Physicochemical properties of C-type starch from root tuber of Apios fortunei in comparison with maize, potato, and pea starches. *Molecules, 23*, 2132.
Wang, Y., Chen, L., Yang, T., Ma, Y., McClements, D. J., Ren, F., … Jin, Z. (2021). A review of structural transformations and properties changes in starch during thermal processing of foods. *Food Hydrocolloids, 113*, Article 106543.
Warren, F. J., Gidley, M. J., & Flanagan, B. M. (2016). Infrared spectroscopy as a tool to characterise starch ordered structure—A joint FTIR–ATR, NMR, XRD and DSC study. *Carbohydrate Polymers, 139*, 35–42.
Wu, D., Ma, H., Fu, M., & Tang, X. (2022). Insight into multi-scale structural evolution during gelatinization process of normal and waxy maize starch. *Journal of Food Science and Technology, 59*, 4405–4414.
Xu, H., Xu, S., Xu, Y., Jiang, Y., Li, T., Zhang, X., Yang, J., & Wang, L. (2024). Relationship between the physicochemical properties and amylose content of rice starch in rice varieties with the same genetic background. *Journal of Cereal Science, 103932*.
Xu, J., Blennow, A., Li, X., Chen, L., & Liu, X. (2020). Gelatinization dynamics of starch in dependence of its lamellar structure, crystalline polymorphs and amylose content. *Carbohydrate Polymers, 229*, Article 115481.
Zhang, S., Fan, X., Lin, L., Zhao, L., Liu, A., & Wei, C. (2017). Properties of starch from root tuber of Stephania epigaea in comparison with potato and maize starches. *International Journal of Food Properties, 20*, 1740–1750.
Zhong, Y., Herburger, K., Xu, J., Kirkensgaard, J. J. K., Khakimov, B., Hansen, A. R., & Blennow, A. (2022). Ethanol pretreatment increases the efficiency of maltogenic α-amylase and branching enzyme to modify the structure of granular native maize starch. *Food Hydrocolloids, 123*, Article 107118.
Zhong, Y., Li, Z., Qu, J., Bertoft, E., Li, M., Zhu, F., Blennow, A., & Liu, X. (2021). Relationship between molecular structure and lamellar and crystalline structure of rice starch. *Carbohydrate Polymers, 258*, Article 117616.
Zhong, Y., Liu, L., Qu, J., Blennow, A., Hansen, A. R., Wu, Y., … Liu, X. (2020). Amylose content and specific fine structures affect lamellar structure and digestibility of maize starches. *Food Hydrocolloids, 108*, Article 105994.
Zhong, Y., Qu, J. Z., Liu, X., Ding, L., Liu, Y., Bertoft, E., … Blennow, A. (2022). Different genetic strategies to generate high amylose starch mutants by engineering the starch biosynthetic pathways. *Carbohydrate Polymers, 287*, Article 119327.
Zhong, Y., Tai, L., Blennow, A., Ding, L., Herburger, K., Qu, J., … Liu, X. (2022). High-amylose starch: Structure, functionality and applications. *Critical Reviews in Food Science and Nutrition*, 1–23.
Zhong, Y., Tian, Y., Liu, X., Ding, L., Kirkensgaard, J. J. K., Hebelstrup, K., … Blennow, A. (2021). Influence of microwave treatment on the structure and functionality of pure amylose and amylopectin systems. *Food Hydrocolloids, 119*, Article 106856.
Zou, J., Xu, M., Tang, W., Wen, L., & Yang, B. (2020). Modification of structural, physicochemical and digestive properties of normal maize starch by thermal treatment. *Food Chemistry, 309*, Article 125733.